APATITE COMPOSITIONS AS A PROXY FOR THE OXIDATION STATES OF PORPHYRY Cu-Mo-Au DEPOSITS

Alexei S. Rukhlov[1], Stephen M. Rowins[1,2], Mao Mao[1], Laurence A. Coogan[2], and Jody Spence[2]

[1]British Columbia Geological Survey, 1810 Blanshard St., Victoria, B.C., V8W 9N3, Canada; [2]School of Earth and Ocean Sciences, University of Victoria, 3800 Finnerty Road, Victoria, British Columbia, V8P 5C2, Canada

Recomended citation:
Rukhlov, A.S., Rowins, S.M., Mao, M., Coogan, L.A. and Spence, J., 2016. Apatite compositions as a proxy for the oxidation states of porphyry Cu-Mo-Au deposits. British Columbia Ministry of Energy and Mines, British Columbia Geological Survey GeoFile 2017-2.

Table 1. Samples

Oxidation state	Type	Name	Age (Ga)	Latitude	Longitude	Sample	Lithology	Apatite grains*	Reference
Oxidized	Abitibi monzonite/syenite suite (ON, Canada)	Cairo stock	2.680	N 48.01	W 80.34	87-SMR-48	Alkali-feldspar syenite	22	Mao et al. (2016)
		McElroy stock	2.705	N 48.05	W 79.48	87-SMR-24	Quartz monzonite	21	
		Murdock Creek stock	2.672	N 48.07	W 80.04	SMR-63	Alkali-feldspar syenite	27	
		Wild Goose Lake pluton	2.713	N 48.24	W 80.30	87-SMR-69	Syenite	22	
		Otto stock	2.678	N 48.04	W 80.02	87-SMR-10	Quartz syenite	22	
						87-SMR-42	Nepheline syenite	21	
						87-SMR-5	Alkali-feldspar syenite	21	
	Alkalic porphyry Cu-Au (BC, Canada)	Mount Polley	0.205	N 52.55	W 121.64	TS3101-2	Foid-bearing syenite	26	
						TS3101-1	Syenite	22	
		Redgold	0.182	N 52.46	W 121.48	TS3901-1	Monzonite	28	
						TS3901-3	Monzonite	10	
	Porphyry Cu-Au (BC, Canada)	Kemess South	0.203	N 57.01	W 126.75	TS2601-2	Quartz monzonite	2	
						TS2601-1	Quartz monzonite	31	
	Porphyry Cu-Mo±Au (BC, Canada)	Brenda	0.194	N 49.88	W 120.01	AP8	Quartz monzonite	23	
		Gibraltar	0.204	N 52.52	W 122.29	TS2201-2	Quartz monzonite	6	
		Highland Valley Copper	0.209	N 50.49	W 121.05	AP9	Granodiorite	8	
		Highmont	0.209	N 50.43	W 121.00	AP7	Alkali-feldspar granite	26	
		Lornex	0.209	N 50.45	W 121.04	AP10	Granodiorite	16	
		Woodjam (Southeast Zone)	0.197	N 52.23	W 121.34	258404	Quartz monzonite	11	Rukhlov et al. (2016)
						258405	Quartz monzonite	10	
	Porphyry Mo (BC, Canada)	Boss Mountain	0.106	N 52.10	W 120.91	AP4	Quartz monzonite	11	Mao et al. (2016)
		Cassiar Moly	0.074	N 59.21	W 129.87	AP5	Greisen	24	
		Endako	0.145	N 54.04	W 125.11	TS1601-2	Quartz monzonite	3	
Intermediate	Porphyry Cu-Au (Michoacán, Mexico)	La Verde	0.033	N 19.08	W 102.03	SMR01-37	Diorite (Mgt- and Ilm-bearing)	17	This study
		San Isidro	0.033	N 18.94	W 101.98	SMR01-46	Granodiorite	23	
						SMR01-50	Quartz monzogabbro	3	
	Porphyry Cu-Mo (BC, Canada)	OK	0.156	N 50.04	W 124.66	OK1118	Leucodiorite (Mgt-bearing)	17	
Reduced	Porphyry Cu-Au	North Fork (Washington, USA)	0.037	N 47.37	W 121.37	SMR01-108	Quartz monzodiorite-granodiorite (Ilm-bearing, I-type)	19	
						SMR01-117	Quartz monzodiorite (Ilm-bearing, I-type)	2	
		San Anton (Guanajuato, Mexico)	0.030	N 21.07	W 101.03	SA98-7-2	Granodiorite (Ilm-bearing, I-type)	20	
		Troilus (QC, Canada)	2.750	N 50.52	W 74.38	KN649-223	Quartz-sulphide vein (Ilm-bearing, I-type)	15	
						SMR05-303	Granite (Ilm-bearing, I-type)	8	
	Porphyry Cu-Mo	Catface (BC, Canada)	0.041	N 49.25	W 125.98	CF1025	Plagioclase-albite porphyry (Ilm-bearing, I-type)	13	
						CF1031	Quartz monzonite, Cliff Zone (Ilm-bearing, I-type)	2	
						CF1013	Quartz monzodiorite, Halo Zone (Ilm-bearing, I-type)	1	

*Number of analyzed apatite grains.

ABSTRACT

A wide range of oxidation states characterize magmatic-hydrothermal systems that form porphyry Cu-Mo-Au deposits. High oxidation states are recognized as an important factor in the genesis of giant porphyry systems, but the wide range of oxidation states that accompany porphyry formation indicates that the role of oxygen fugacity in the ore-forming process is complex. Previous studies have shown that concentrations of multivalent elements S, V, Cr, Mn, Fe, Ga, As, Ce, and Eu in apatite can be used as redox sensors in magmas and fluids. Here we follow up the utility of apatite chemistry as a redox proxy using both new and published electron microprobe (n = 528) and laser-ablation inductively coupled plasma mass spectrometry (n = 570) data from five Neoarchean monzonite-syenite plutons of the southern Abitibi belt and nineteen porphyry Cu-Mo-Au deposits with oxidation states ranging between ΔFMQ = -3 to +3, based on independent estimates from petrologic buffers. Apatites from reduced, ilmenite-bearing, calc-alkaline porphyry systems (e.g., Catface, North Fork, San Anton, Troilus) have much lower S, V, and Eu contents than those of oxidized monzonite-syenite intrusions and alkalic porphyry Cu-Au systems (e.g., Mount Polley, Redgold). Apatites from oxidized, magnetite-bearing, calc-alkaline porphyry Cu±Mo±Au (e.g., Kemess, Highland Valley) and porphyry Mo (e.g., Boss Mountain, Endako) systems have intermediate contents of these elements. These elements in apatite appear to correlate with the oxidation state of the magmas. Concentrations of Mn, As, and Ce vary up to three orders of magnitude between individual deposits suggesting additional controls of their behavior.

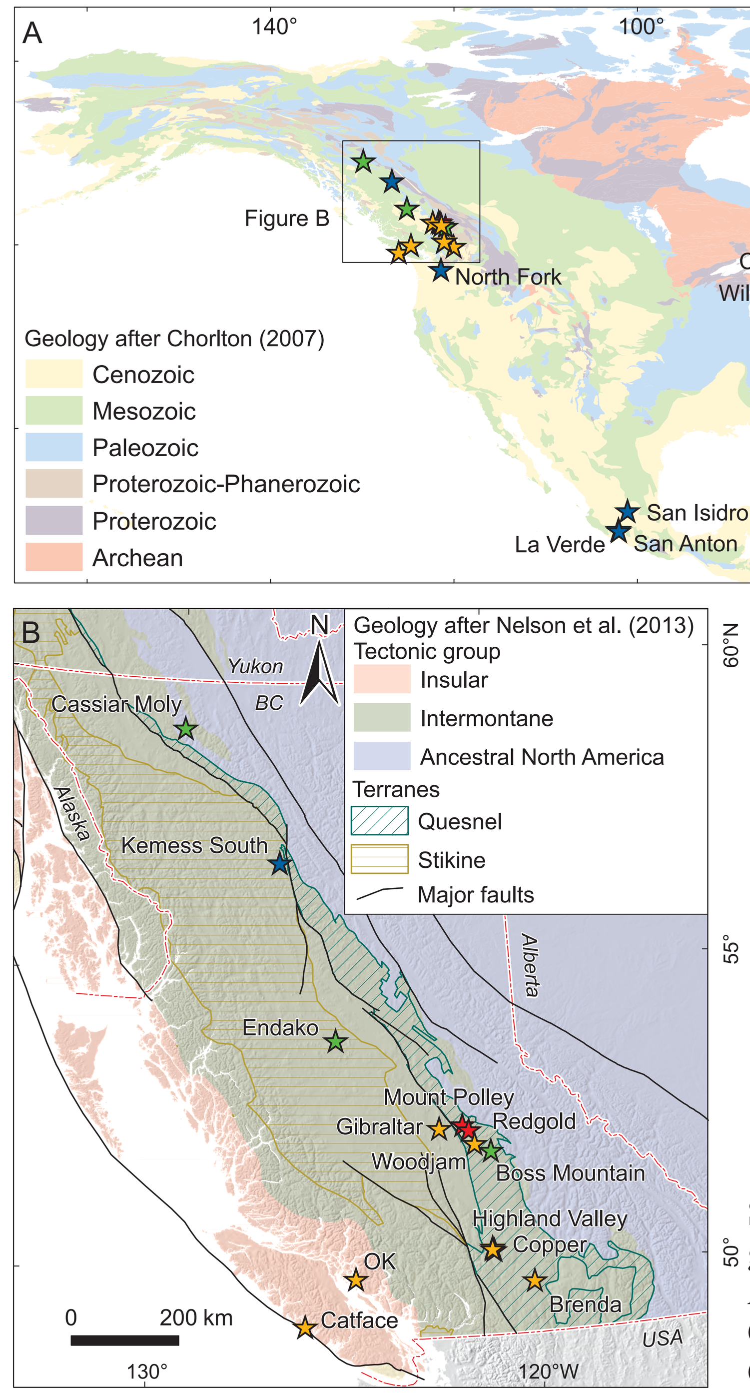

Sample locations and geology. A: North America. B: Northern Cordillera, British Columbia, Canada.

OXIDIZED SYSTEMS

Abitibi suite (ON, Canada)
- Alkali-feldspar syenite, Cairo
- Quartz monzonite, McElroy
- Alkali-feldspar syenite, Murdock Creek
- Alkali-feldspar syenite — Otto
- Nepheline syenite — Otto
- Quartz syenite — Otto
- Syenite, Wild Goose Lake

Alkalic porphyry Cu-Au (BC, Canada)
- Foid-bearing syenite — Mount Polley
- Syenite — Mount Polley
- Monzonite, Redgold

Porphyry Cu-Au (BC, Canada)
- Quartz monzonite, Kemess South

Porphyry Cu-Mo±Au (BC, Canada)
- Quartz monzonite, Brenda
- Quartz monzonite, Gibraltar
- Granodiorite, Highland Valley Copper
- Alkali-feldspar granite, Highmont
- Granodiorite, Lornex
- Quartz monzonite, Woodjam (Southeast Zone)

Porphyry Mo (BC, Canada)
- Quartz monzonite, Boss Mountain
- Greisen, Cassiar Moly
- Quartz monzonite, Endako

INTERMEDIATE SYSTEMS

Porphyry Cu-Au (Michoacán, Mexico)
- Diorite, La Verde
- Granodiorite — San Isidro
- Quartz monzogabbro — San Isidro

Porphyry Cu-Mo (BC, Canada)
- Leucodiorite, OK

REDUCED SYSTEMS

Porphyry Cu-Au
- Quartz monzodiorite — North Fork (Washington, USA)
- Quartz monzodiorite-granodiorite — North Fork (Washington, USA)
- Granodiorite, San Anton (Guanajuato, Mexico)
- Granite — Troilus (QC, Canada)
- Quartz-sulphide vein — Troilus (QC, Canada)

Porphyry Cu-Mo (Catface, BC, Canada)
- Plagioclase-albite porphyry
- Quartz monzodiorite, Halo Zone
- Quartz monzonite, Cliff Zone

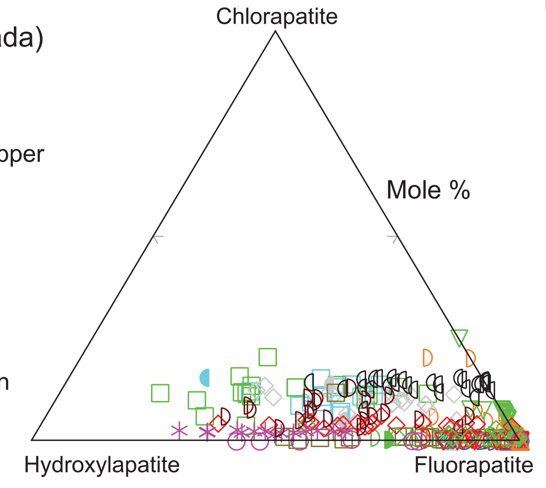

Apatite ternary assuming that F, Cl, and OH fill the halogen-site in apatite.

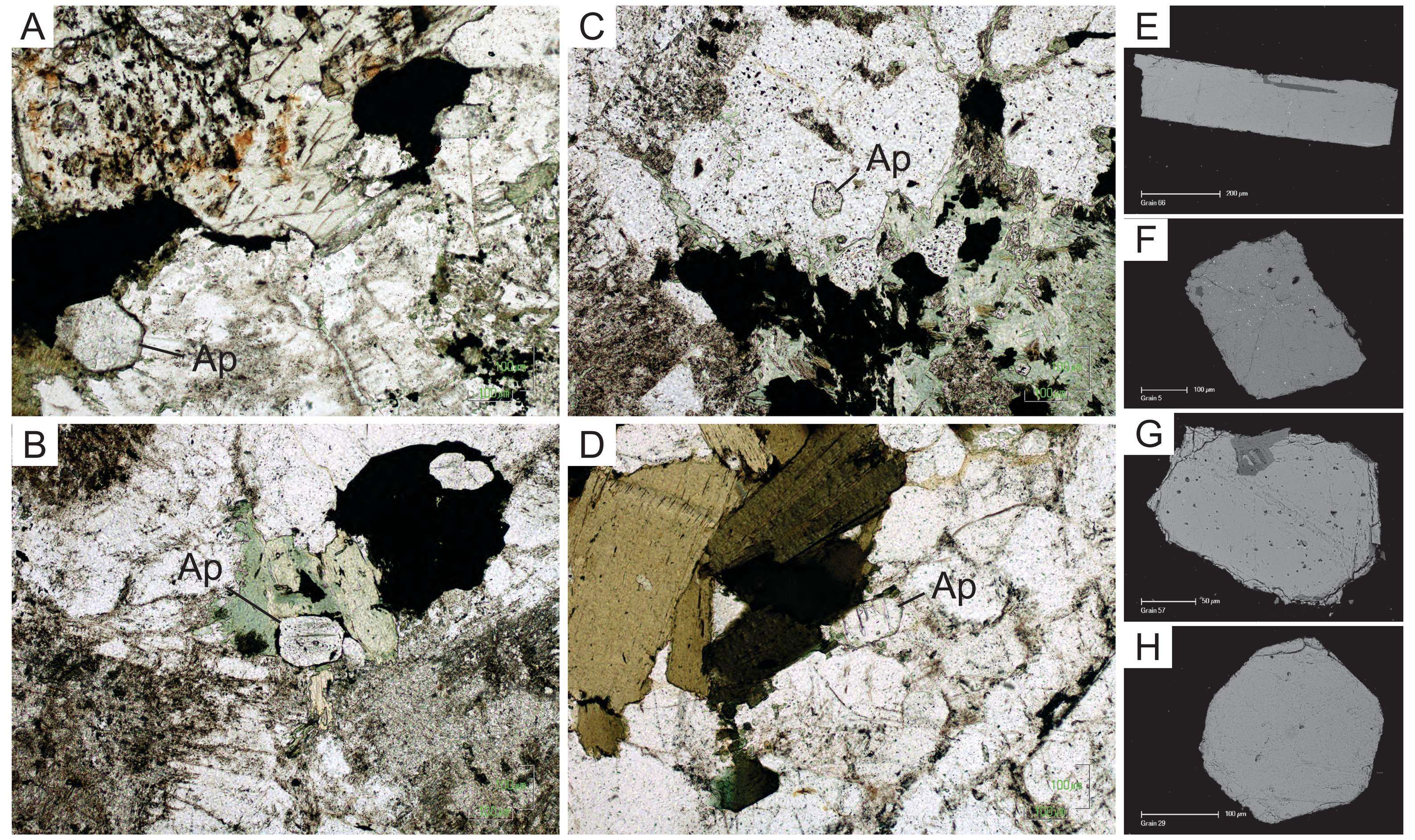

Photomicrographs (A-D) and BSE images of apatites (E-H) from La Verde diorite, sample SMR01-37 (A, E); OK leucodiorite, sample OK1118 (B, F); North Fork quartz monzodiorite-granodiorite, sample SMR01-108 (C, G); and Catface quartz monzodiorite, samples CF1014 (D) and CF1025 (H).

SAMPLES AND METHODS

Rock samples (Table 1) were examined in thin sections before crushing and apatite separation using heavy liquids, hand magnet and Frantz isodynamic separator at the British Columbia Geological Survey. Apatite grains were hand-picked from the 0.18–0.50 mm, 2.97-3.32 $g\cdot cm^{-3}$, >1.5 A fraction under a binocular microscope. Recovered apatite grains were individually checked by qualitative energy-dispersive X-ray spectroscopy (EDS) using PKα and CaKα X-ray lines on a Thermo Scientific NITON® FXL 950 portable X-ray fluorescence (XRF) spectrometer. Confirmed apatite grains (up to 23 per sample) were mounted in epoxy, polished and analyzed by a Cameca SX50 electron probe microanalyzer (EPMA) in wavelength dispersion mode for F, Na, Si, P, S, Cl, Ca and Fe at the Department of Earth, Ocean and Atmospheric Sciences, University of British Columbia. The average precision (2σ relative %) based on counting statistics was 1.2% for Ca, 3.7% for P, 41% for F, 85% for Cl, 204% for Si, 238% for Na, 360% for S, and 345% for Fe. The average relative difference on duplicate analyses of 5 apatite grains was 0.8% for Ca, 2.6% for P, 11% for Cl, 22% for F, 49% for S, 52% for Fe, 65% for Si, and 76% for Na. Backscatter secondary electron (BSE) images were obtained for each apatite grain on a Philips XL30 electron microscope in the same laboratory. Thirty-two trace elements (Z=12 to 92) were analyzed on a Thermo X-Series II (X7) quadrupole inductively coupled plasma mass spectrometer (ICP-MS) equipped with a New Wave UP-213 laser ablation (LA) system using He as the carrier gas at the School of Earth and Ocean Sciences, University of Victoria. Detection limits and the statistics on quality controls are summarized in Table 2, and full details of the analytical procedures can be found in Mao et al. (2016) and Rukhlov et al. (2016). In addition, we used selected apatite compositions from our published database (Mao et al., 2016; Rukhlov et al., 2016).

Table 2. LA-ICPMS detection limits and quality controls.

Analyte (ppm)	Detection limit (DL) range*	Durango reference apatite					Madagascar reference apatite					NIST 611				NIST 613				NIST 615			
		N	N<DL	Mean	σ	Mao et al. (2016)	N	N<DL	Mean	σ	Mao et al. (2016)	N	N<DL	Mean	σ	N	N<DL	Mean	σ	N	N<DL	Mean	σ
^{25}Mg	20-64	31	0	125	4	124(30)	31	0	59	5	53(29)	31	0	432	15	31	0	57	7	31	0	25	4
^{49}Ti	1.9-43	20	15	<0.6			19	16	<1.4			31	0	448	13	31	0	37	7	31	0	4.5	9.7
^{51}V	1.1-6	31	0	43.0	4.3	43(16)	31	0	28.9	2.0	26(10)	31	0	439	10	31	0	37.3	1.3	31	0	0.91	0.22
^{55}Mn	4.8-25	31	0	94.8	3.1	97(8)	31	0	252	7	251(19)	31	0	434	10	31	0	37.1	1.1	25	6	0.81	0.40
^{57}Fe	50-321	31	0	372	35		31	0	202	35		31	0	442	15	31	0	73.4	10.1	31	0	43	12
^{65}Cu	1.4-20	25	15	<0.22		<3.4	22	13	<1.3		<0.35	31	0	428	15	31	0	37.9	6.3	29	2	1.26	0.26
^{66}Zn	2.5-4.3	21	15	<0.26		<2.7	21	12	<1.3		<1.8	31	0	456	15	31	0	39.8	5.5	31	0	3.5	4.4
^{75}As	6.3-38	31	0	1175	175	1242(271)	31	0	13.6	1.9	13(11)	31	0	326	20	31	0	33.3	1.9	31	0	0.71	0.22
^{85}Rb	0.68-2.2	10	24	<0.1		<1.0	14	18	<1.5		<0.6	31	0	425	8	31	0	31.2	0.8	31	0	0.86	0.05
^{88}Sr	2.1-13	31	0	508	11	513(29)	31	0	1997	47	2001(112)	31	0	516	7	31	0	78.6	1.4	31	0	45.5	1.0
^{89}Y	2.6-20	31	0	657	33	670(98)	31	0	279	6	276(37)	31	0	461	6	31	0	38.7	0.7	25	8	0.69	0.15
^{90}Zr	0.67-2.3	29	2	0.43	0.19	<0.53	31	0	19	2	16(5)	31	0	450	6	31	0	38.9	0.9	31	0	0.84	0.08
^{93}Nb	0.7-2.2	15	20	<0.1		<0.12	22	14	<1.0		<0.12	31	0	462	8	31	0	38.1	0.7	31	0	0.80	0.05
^{95}Mo	0.73-2.2	13	22	<0.1		<0.81	22	15	<1.0		<0.81	31	0	415	9	31	0	36.0	1.4	31	0	0.76	0.10
^{137}Ba	0.73-2.2	31	0	1.6	0.4	<1.4	28	6	<1.1		<0.32	31	0	460	8	31	0	40.1	1.2	31	0	3.36	0.22
^{139}La	4.6-18	31	0	3907	77	3879(326)	31	0	2099	39	2058(176)	31	0	445	6	31	0	36.5	0.8	27	4	0.61	0.24
^{140}Ce	9.2-40	31	0	4738	198	4773(396)	31	0	4381	247	4309(607)	31	0	457	7	31	0	38.1	0.9	23	8	0.64	0.31
^{141}Pr	1.6-6	31	0	367	7	368(26)	31	0	445	10	435(26)	31	0	454	7	31	0	38.2	0.8	30	3	0.72	0.15
^{146}Nd	5.1-25	31	0	1177	24		31	0	1521	33		31	0	437	9	31	0	36.0	1.1	25	6	0.69	0.32
^{147}Sm	1.2-6.1	31	0	166	6	162(22)	31	0	199	6	186(26)	31	0	461	8	31	0	38.7	1.1	29	2	0.69	0.24
^{153}Eu	0.7-2.3	31	0	15.9	0.5	16(2)	31	0	29.2	1.9	27(4)	31	0	456	8	31	0	36.3	0.9	31	0	0.73	0.06
^{157}Gd	1.1-5.9	31	0	151	7	149(21)	31	0	123	4	118(15)	31	0	458	9	31	0	39.1	1.1	31	2	0.74	0.22
^{163}Dy	0.82-4.3	31	0	108	7	107(16)	31	0	59.4	2.4	56(8)	31	0	449	9	31	0	37.0	0.9	31	0	0.70	0.18
^{165}Ho	0.64-2.2	31	0	21.4	1.3		31	0	10.4	1.7		31	0	461	10	31	0	39.3	0.9	31	0	0.75	0.05
^{172}Yb	0.7-2.7	31	0	40.7	1.7	39(6)	31	0	16.6	1.8	15(4)	31	0	461	10	31	0	39.8	0.9	31	0	0.73	0.08
^{175}Lu	0.6-2.1	31	0	4.8	0.3		31	0	2.6	1.6		31	0	453	10	31	0	38.1	1.1	31	0	0.74	0.04
^{182}W	0.63-2.1	15	19	<0.04		<0.017	23	15	<1.0		<0.048	31	0	450	9	31	0	38.1	1.2	31	0	0.79	0.06
^{208}Pb	0.62-2.1	30	1	0.62	0.17	<0.9	31	0	29.2	1.9	26(5)	31	0	439	11	31	0	38.8	1.2	31	0	2.30	0.12
^{232}Th	1.2-4.3	31	0	230	24	220(42)	31	0	638	17	599(104)	31	0	471	9	31	0	39.1	1.1	31	0	0.74	0.06
^{238}U	0.65-2.3	31	0	10.4	0.4	10(2)	31	0	25.0	2.1	23(5)	31	0	474	11	31	0	38.0	1.2	31	0	0.84	0.04

* Signal (average + 3σ) before ablation, calibrated for internal standard, instrument drift, and sensitivity.

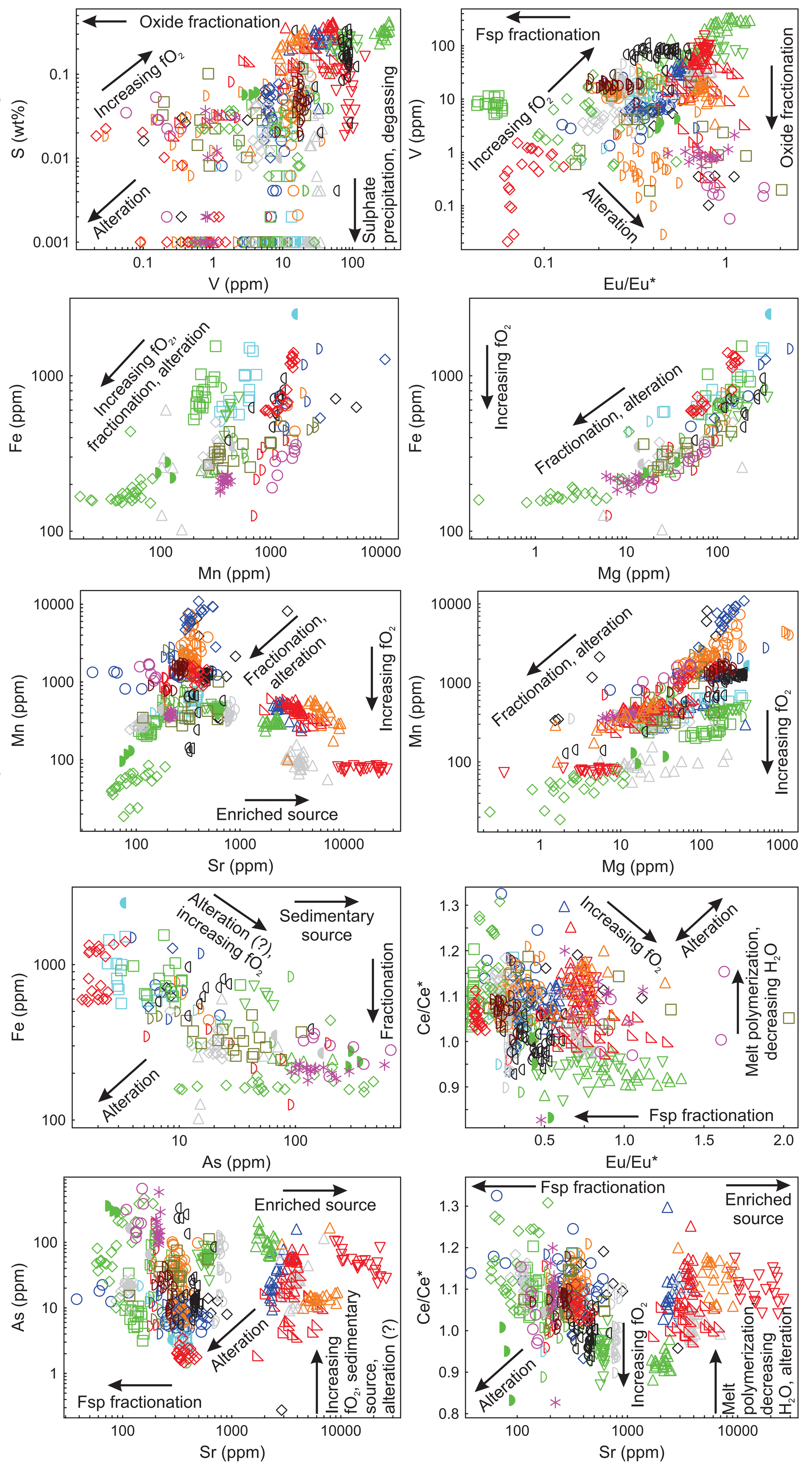

Scatter plots for trace elements in apatite showing various local controls of their behaviour.

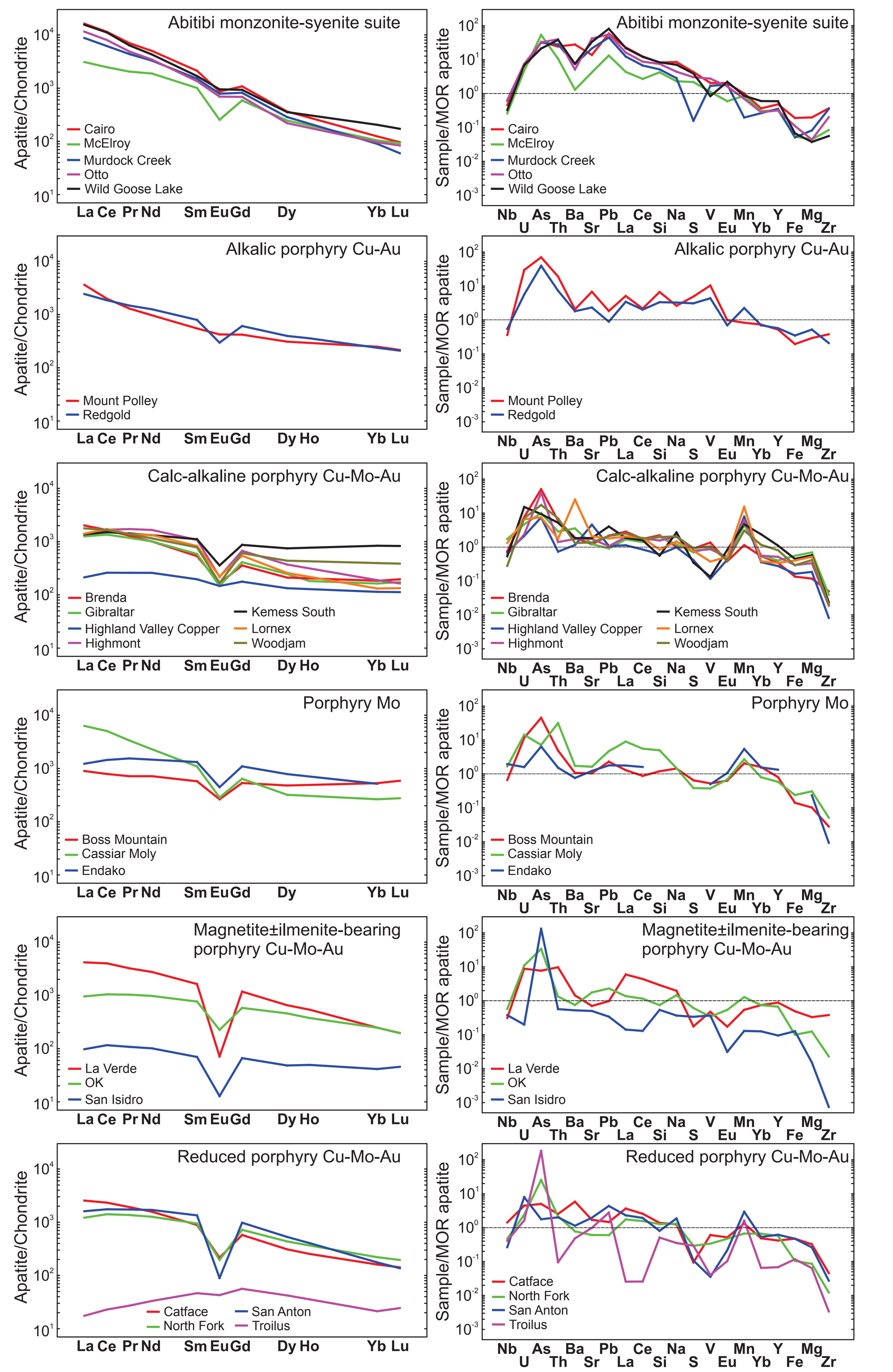

Average apatite compositions; mid-ocean ridge (MOR) apatite after Mao et al. (2016)

SUMMARY

- Abundances of multivalent elements S, V, Mn, Fe, As, Ce, and Eu in apatite are controlled by source heterogeneity, oxidation state, bulk composition, and crystallization history of a parental magma-fluid, and alteration.
- S, V, and Eu contents in apatite correlate with the oxidation state of the magmas.
- Coupled Mn and Fe variations also distinguish Abitibi monzonite-syenite suite and porphyry Cu-Mo-Au systems with oxidation states ranging between ΔFMQ = -3 to +3, based on estimates from petrologic buffers.

REFERENCES

Chorlton, L.B., 2007. Generalized geology of the world: bedrock domains and major faults in GIS format. Geological Survey of Canada, Open File 5529, CD-ROM.

Mao, M., Rukhlov, A.S., Rowins, S.M., Spence, J., and Coogan, L.A., 2016. Apatite trace-element compositions: A robust new tool for mineral exploration. Economic Geology, 111, pp. 1187–1222.

Nelson, J.L., Colpron, M., and Israel, S., 2013. The Cordillera of British Columbia, Yukon and Alaska: tectonics and metallogeny. In: Colpron, M., Bissig, T., Rusk, B.G., and Thompson, F.H. (Eds.), Tectonics, Metallogeny, and Discovery: The North American Cordillera and Similar Accretionary Settings, Society of Economic Geologists, Inc. Special Publication 17, pp. 53–109.

Rukhlov, A.S., Plouffe, A., Ferbey, T., Mao, M., and Spence, J., 2016. Application of trace-element compositions of detrital apatite to explore for porphyry deposits in central British Columbia. In: Geological Fieldwork 2015, British Columbia Ministry of Energy and Mines, British Columbia Geological Survey Paper 2016-1, pp. 145-179.